Lifetime Spectroscopy of FeB Pairs in Silicon

Daniel Macdonald and Andres Cuevas
Center for Sustainable Energy Systems, Dept. of Engineering, FEIT
Australian National University, Acton, ACT 0200, Australia

Abstract – Injection-level dependent lifetime curves of iron-contaminated silicon wafers of various resistivities have been modeled using Shockley-Read-Hall theory. The modeling allows accurate determination of the capture cross-sections of FeB pairs. These cross-sections are then used to extend the validity of a commonly used method for determining iron concentrations to all resistivities. The impact of interstitial iron on solar cell parameters is also modeled and discussed.

1. INTRODUCTION

Iron is an important impurity in silicon devices, whether for photovoltaic or microelectronic applications. As such, it is desirable to characterize the electronic properties of its common forms as accurately as possible. While this has largely been achieved for interstitial iron (Fe_i), it has not fully occurred for the acceptor level of FeB pairs. The energy level of the latter has been determined by deep-level transient spectroscopy (DLTS) with reasonable accuracy, but measurement of the capture cross-sections has to date been uncertain [1].

This paper presents a new technique, known as Injection-level Dependent Lifetime Spectroscopy (IDLS), for accurately determining these properties. The method is based on modeling lifetime measurements on samples with widely varying dopant densities, with Shockley-Read-Hall (SRH) statistics. In terms of determining carrier capture cross-sections, it is more accurate than conventional techniques such as DLTS.

The results have implications for widely used techniques for measuring the iron concentration based on the change in diffusion length after thermal dissociation of FeB pairs [2]. The scaling factors used in these methods are in fact resistivity dependent, a fact that is not always recognised. The cross-sections of FeB pairs determined in this study by IDLS have allowed these factors to be calculated for any resistivity.

Finally, in operating solar cells, all of the non-precipitated Fe will be present as Fe_i. Using the known energy level and capture cross-sections of this impurity, the impact of varying levels of Fe_i on the I-V curve of a silicon cell can be modeled. One interesting consequence is that the strong asymmetry of the cross-sections results in degradation of the fill factor, even for relatively low Fe_i concentrations.

2. LIFETIME SPECTROSCOPY OF FeB PAIRS IN SILICON

As summarized recently by Istratov *et al.* [1], there exist two charge states of the FeB pair in silicon. One state occurs as a donor level at E_V+0.1eV, and the other as an acceptor level at E_C-0.26(±0.03)eV. Brotherton *et al.* [3] argued that the acceptor level must be the dominant recombination center of the two, due to the fact that it is deeper. Hayamizu *et al.* [4] showed that the acceptor level does indeed dominate recombination through FeB pairs at room temperature. They performed temperature dependent low-injection lifetime measurements, which could only be adequately described by a relatively deep level around 0.29eV from either band edge.

In another study, Walz *et al.* [5] examined the injection-level dependence of the recombination lifetimes at room temperature of iron-diffused samples for a range of intermediate resistivities, and found that their data could be adequately explained by modeling the combined effect of the acceptor level and the level for interstitial iron. They were able to determine values for the capture cross-sections of the acceptor level by fitting SRH curves. This technique,

referred to here as Injection-level Dependent Lifetime Spectroscopy (IDLS) [6], can allow more accurate measurement of cross-sections than the more commonly used DLTS methods, which require extrapolation of emission rate data to an axis. However, a crucial requirement of the IDLS technique is that samples with widely different dopant densities need to be used. The important feature of these different resistivities is that the injection-level dependence of the lifetime for a given defect is often markedly different, allowing accurate fitting of SRH curves with a consistent and unique pair of capture cross-sections. Walz *et al.*'s study was restricted to a resistivity range of 1 to 20Ωcm due to constraints of their measurement method (ELYMAT). In this work, we study a larger range of resistivities, from 0.3 to 150Ωcm. This corresponds to 25 times the dopant density range used by Walz *et al.*, a feature that turns out to be very important for *uniquely* determining the cross-sections.

In addition to varying the dopant densities, the dissociation behavior of FeB pairs upon illumination may be used to vary the recombination center densities by applying different levels of light-soaking. In our experiments, the total iron concentration is known from the implantation dose, and so the sum of the modeled FeB and Fe_i centers can be forced to equal this value. In this way, a good fit can be achieved for each light-soaking condition and resistivity, resulting in uniquely determined capture cross-sections.

2.1 Experimental Methods

Care needs to be taken during sample preparation to ensure that the deliberately introduced Fe occurs evenly throughout the bulk of the wafers, as this is essential for accurate injection-level dependent lifetime measurements. Also, the impurities to be studied should not be subject to significant gettering at the surfaces or damaged regions, nor undergo excessive out-diffusion or precipitation in the bulk. In this study, avoiding loss of iron through these processes allows us to determine the bulk iron concentration, after annealing, from a knowledge of the implantation dose. This is important in modeling the lifetime data and allowing the accurate fitting of the SRH parameters.

Boron-doped *p*-type float zone (FZ) silicon samples of four resistivities (0.3, 1, 5 and 150Ωcm) were chosen for this study. The exact details of their preparation is given elsewhere [7]. In summary, they were implanted with 70keV ^{56}Fe and annealed at 900°C for 1 hour to distribute the iron uniformly throughout the wafers. Surface passivation was achieved by depositing films of plasma-enhanced chemical vapor deposited (PECVD) silicon nitride [8]. This passivation allows lifetimes of above 1ms to be observed in high resistivity material.

The quasi-steady-state photoconductance (QSSPC) technique[9] was used to measure the injection-level dependence of the effective lifetimes. Control samples were included to ensure that the measured lifetimes reflected the recombination properties of the iron-related states only, and not surface effects or the pre-implanted lifetime of the FZ wafers. This was confirmed by the fact that the effective lifetimes measured on the control samples were almost always an order of magnitude or more greater than the lifetimes of the iron implanted samples.

2.2 Shockley-Read-Hall Statistics

The injection-level dependence of the SRH lifetime τ_{SRH} is a function of the dopant density N_A, recombination center density N_{SRH}, defect energy level E_T and capture cross-sections, and for *p*-Si is given by[10-12]:

$$\frac{1}{\tau_{SRH}} = \frac{N_A + \Delta n}{\tau_{p0}(n_1 + \Delta n) + \tau_{n0}(N_A + p_1 + \Delta n)} \qquad (1)$$

Here, $\Delta n = \Delta p$ is the excess carrier density, and τ_{n0} and τ_{p0} are the fundamental electron and hole lifetimes, which are related to the recombination center density, the thermal velocity[13] $v_{th}=1.1\times10^7 cms^{-1}$, and the capture cross-sections via $\tau_{n0}=1/(v_{th}\sigma_n N_{SRH})$ and $\tau_{p0}=1/(v_{th}\sigma_p N_{SRH})$. The statistical factors n_1 and p_1 are the electron and hole densities when the Fermi energy coincides with the recombination center energy [12].

Under low- ($\Delta n << N_A$) and high-injection ($\Delta n >> N_A$) conditions, Eq. 1 can be simplified for a given

Recom. Center	Energy (eV)	σ_n , σ_p (cm^{-2})	Low-inj. τ_{SRH}	High-inj. τ_{SRH}
Fe_I (ref [1])	E_V+0.38	5×10^{-14} 7×10^{-17}	τ_{n0}	τ_{p0}
FeB (this work)	E_C-0.23	3×10^{-14} 2×10^{-15}	$\tau_{p0}(n_1/N_A)$ $+\tau_{n0}$	τ_{p0}
FeB (Walz)	E_C-0.29	2.5×10^{-15} 3×10^{-14}	τ_{n0}	τ_{n0}

TABLE 1. Energy levels, capture cross-sections, and approximations for the SRH lifetimes under low- and high-injection for Fe_i and FeB pairs.

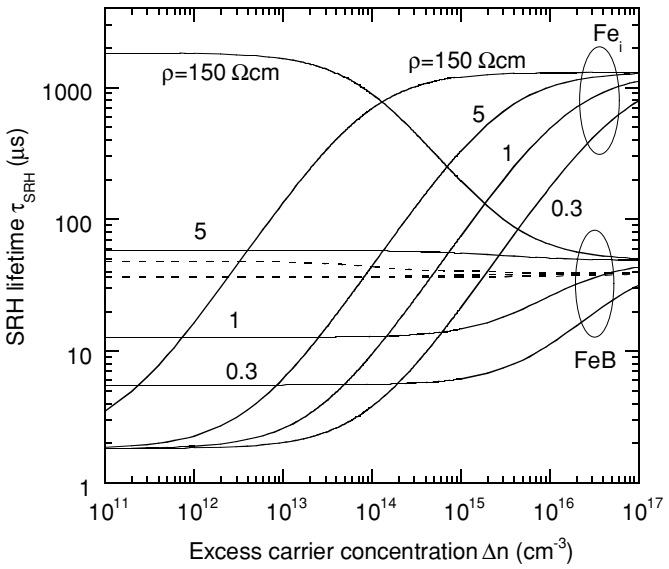

FIGURE 1. SRH lifetime curves for different Fe-related recombination centres in p-type silicon of different resistivities. Curves for FeB using Walz et al.'s values are shown as dashed lines. The lower dashed line represents the three lower resistivities, which coincide.

recombination center. These are listed in Table 1 for three cases: interstitial iron, FeB pairs with the recombination parameters used in this work, and FeB pairs with those used by Walz.

Fig 1 illustrates theoretical injection-level dependent lifetime curves for these three cases. The curves, calculated for a bulk defect concentration of $1\times10^{12}cm^{-3}$ for each of the four resistivities used in this study, reveal their different behaviors. Note in particular the lack of injection-level dependence of Walz's parameters for the FeB pair in comparison with those used in this study. However, as mentioned, Walz only measured samples in a small range of resistivities, from 1 to 20Ωcm, and over this narrow

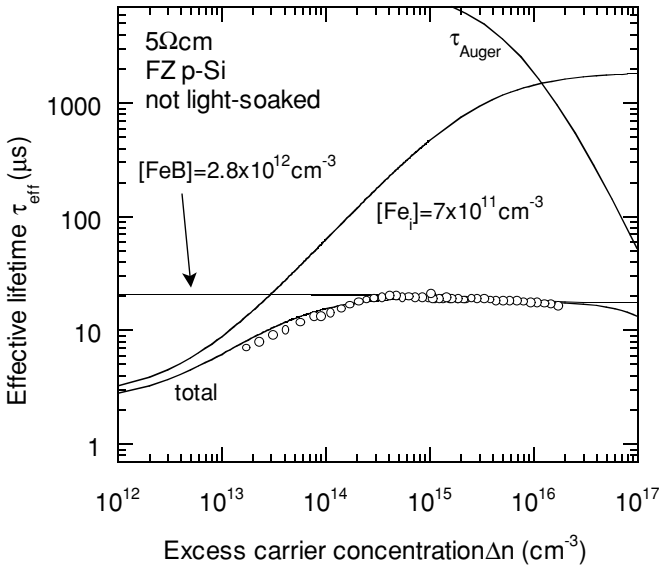

FIGURE 2. Fitting procedure for the 5Ωcm sample without light-soaking. The implanted dose was $1\times10^{11}cm^{-2}$.

range the optimum parameters found in this current study also give a mild dependence. Hence, the parameters found in this work, and those found by Walz, provide reasonable approximations to one another over the narrower dopant range. However, when data from a much larger dopant density range is examined, the cross-sections determined in this study must be used.

2.3 Modeling Procedure

The effects of Auger recombination are often important in heavily doped or highly excited silicon[14], and need to be considered here at the higher carrier concentrations. The control samples reveal that the surfaces are not significant in the iron-diffused samples studied. Therefore, the effective lifetime, comprising all of the important contributions, can be expressed as:

$$\frac{1}{\tau_{eff}} = \frac{1}{\tau_{SRH}^{Fe_i}} + \frac{1}{\tau_{SRH}^{FeB}} + \frac{1}{\tau_{Auger}} \qquad (2)$$

The Auger lifetime is calculated using a Coulomb-enhanced Auger recombination model [15,16] which is valid for all injection-levels and dopant densities. Values for the Auger coefficients C_n, C_p and C_a are taken from the literature [14,17].

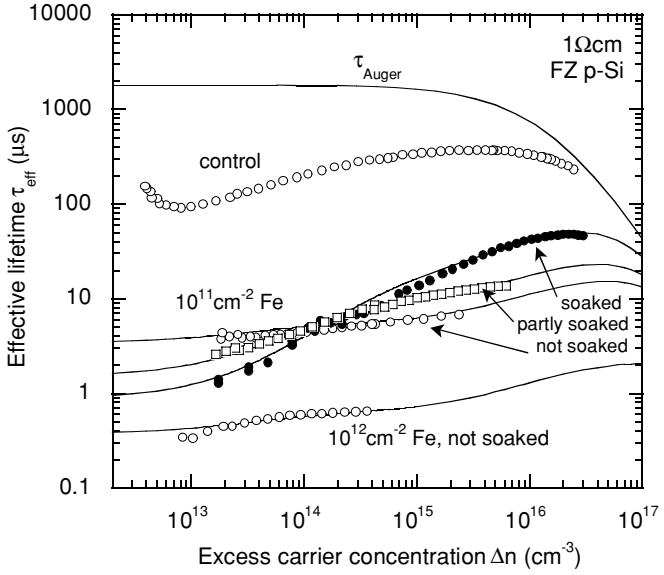

FIGURE 3. Lifetime measurements and SRH fits for 1Ωcm samples implanted with iron doses of $1\times10^{11}cm^{-2}$ and $1\times10^{12}cm^{-2}$.

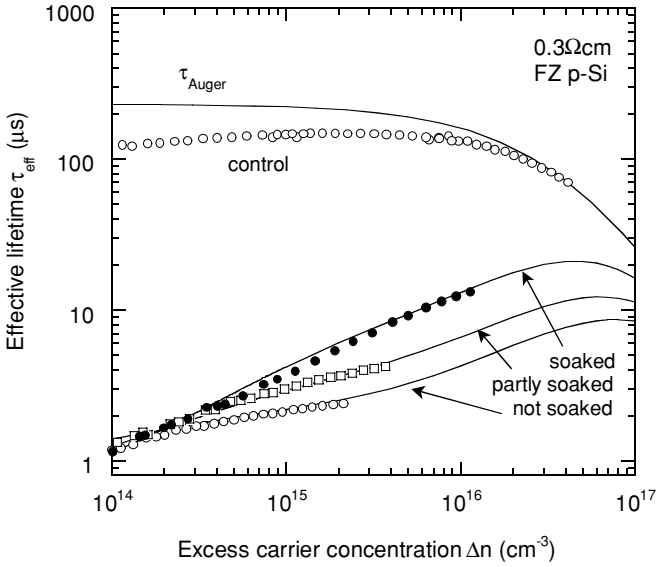

FIGURE 4. Lifetime measurements and SRH fits for the 0.3Ωcm sample implanted with an iron dose of $1\times10^{11}cm^{-2}$.

The fitting procedure proceeds as follows. Curves such as those in Fig 1 are taken for interstitial iron and FeB pairs for the appropriate resistivity. These curves are combined in a linear fashion according to Eq. 2, with a term for Auger recombination included, and compared to the measured data. The concentrations of each center are adjusted, and the shape of the FeB curve altered by changing the cross-sections, until a good fit is obtained for all the samples with a single set of cross-sections. An example of the fitting process are given in Fig 2. In this figure, data for the 5Ωcm sample without light-soaking is shown, and is dominated by the presence of FeB pairs.

For all samples, the sum of the modeled interstitial iron and FeB pair concentrations is forced to agree with that expected from the implantation dose. For Fig 2, this sum equals $3.5\times10^{12}cm^{-3}$, precisely that expected from an implant dose of $1\times10^{11}cm^{-2}$ in a wafer of thickness 0.0285cm.

2.4 Results and Discussion

Figure 3 depicts the results for two 1Ωcm, iron implanted samples, with doses of 1×10^{11} and $1\times10^{12}cm^{-2}$. There are three curves for the lighter dose corresponding to different light-soaking levels,

Resistivity (Ωcm)	[Fe] (cm^{-3}) from dose	Light soaking	Modeled [Fe_i] (cm^{-3})	Modeled [FeB] (cm^{-3})
0.3	3.5×10^{12}	none	1.0×10^{12}	2.5×10^{12}
〃	〃	partial	2.0×10^{12}	1.5×10^{12}
〃	〃	full	2.9×10^{12}	0.6×10^{12}
1	2.5×10^{12}	none	0.2×10^{12}	2.3×10^{12}
〃	〃	partial	1.1×10^{12}	1.4×10^{12}
〃	〃	full	2.0×10^{12}	0.5×10^{12}
〃	2.5×10^{13}	none	0.2×10^{13}	2.0×10^{13}
5	3.5×10^{12}	none	0.7×10^{12}	2.8×10^{12}
150	2.9×10^{13}	none	0.5×10^{13}	2.0×10^{13}

TABLE 2. Modeled and implanted iron concentrations for the different resistivity samples under different light-soaking conditions.

and hence different relative populations of Fe_i and FeB pairs. The fact that these concentrations add to agree with that expected from the dose, as shown in Table 2, indicates that very little precipitation has occurred in the samples. This is further corroborated by the fact that a good fit for the heavier dose can be achieved by merely scaling up the concentrations by an order of magnitude. It is interesting to note that even in the fully light-soaked case, it was still necessary to include a small number of FeB pairs to describe the data well, indicating that either pair dissociation is not complete or that some re-pairing

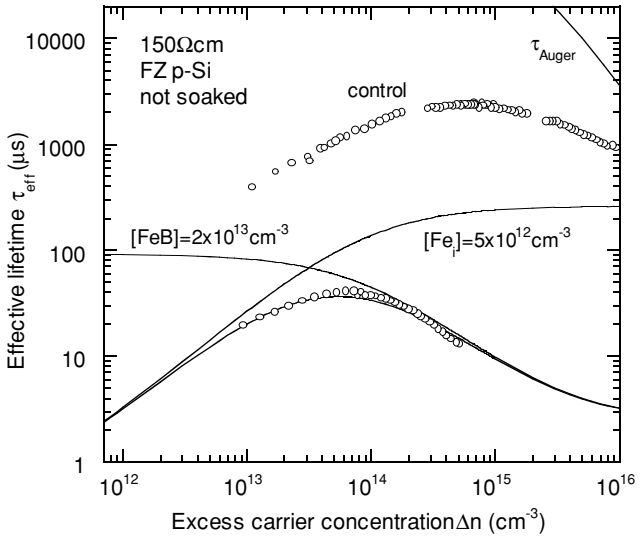

FIGURE 5. Lifetime measurements and SRH fits for the 150Ωcm sample implanted with an iron dose of 1×10^{12}cm^{-2}.

occurs between light-soaking and lifetime measurement.

Figure 4 shows the results for the 0.3Ωcm sample, implanted with a dose of 1×10^{11}cm^{-2}. Once again, the sum of the modeled concentrations agrees well with that obtained from the dose. For the 150Ωcm light-soaked case, the dependence becomes much more pronounced, as revealed in Fig 5. In this plot, the constituent SRH curves for the FeB pairs and Fe_i are also shown. The strong dependence of the FeB curve is clear in this case, which contrasts with the weak dependence predicted by Walz's cross-sections (see Fig 1). Note that in comparison with the 0.3Ωcm data in Fig 4, the lifetime dependence without light-soaking goes in opposite directions as the carrier density increases, again as expected from Fig 1.

The data in Fig 5 is for a sample that was implanted with a heavier dose of 1×10^{12}cm^{-2}. For this resistivity, the corresponding wafer with the lighter dose gave lifetime data that was too close to the control sample, meaning that surface recombination impacted on the measurements.

For the fits shown, the capture cross-sections used for the FeB pairs were $\sigma_n=3\times10^{-14}$cm^{-2} and $\sigma_p=2\times10^{-15}$cm^{-2}. It is possible to estimate the uncertainty in these values by adjusting them and observing the effect on the fits. In conjunction with a typical uncertainty in the measured lifetimes of around 20%, and an uncertainty of about 5% in the dopant densities, we can state that the cross-sections should reside in the ranges $\sigma_n=(3\pm2)\times10^{-14}$cm^{-2} and $\sigma_p=(2\pm1)\times10^{-15}$cm^{-2}. The value of the energy level used was Ec-0.23eV, which is within the uncertainty bounds reported by Istratov in his recent review of iron complexes in silicon[1].

As a more general observation, this work illustrates that with appropriate choices of implant dose, annealing temperature and time, and a good range of substrate resistivities, injection-level dependent lifetime spectroscopy offers an accurate alternative to DLTS techniques for determining capture cross-sections of defects in semiconductors, especially if the defect energy is known.

3. RATIO AND DIFFERENCE OF DIFFUSION LENGTHS

Zoth and Bergholz [2] found that samples dominated by Fe_i and FeB pairs could be identified by the ratio of the diffusion lengths L_1/L_0, as measured by the Surface Photovoltage method (SPV), before (L_0) and after (L_1) thermal annealing at 210ºC. Prior to annealing, the majority of the Fe is in the form of FeB pairs, whilst after annealing it is present as Fe_i. Due to constraints of the technique, SPV measurements are always performed under low-injection conditions. Since the low-injection lifetime of Fe_i is independent of the dopant density, while for FeB pairs it depends strongly on the dopant density, it follows that the ratio of the diffusion lengths is also a function of N_A. Indeed, Zoth and Bergholz found that this was true, and they reported the value of L_1/L_0, to be about 0.5, 0.33 and 0.25 for dopant densities of 10^{16}, 10^{15} and $<5\times10^{14}$cm^{-3}.

Using the energy level and cross section data from the previous section, it is possible to calculate the diffusion length ratio L_1/L_0 as a function of the dopant density using the SRH model. Figure 6 shows the results, with Zoth and Bergholz's SPV data included for comparison. The error bars for their experimental points are only estimates. Also shown

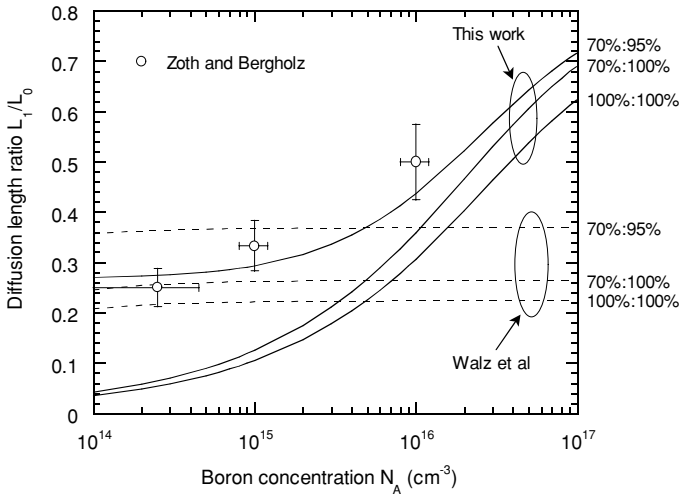

FIGURE 6. Diffusion length ratio (low-injection) after and before thermal annealing for iron-dominated p-*type samples as a function of dopant density.*

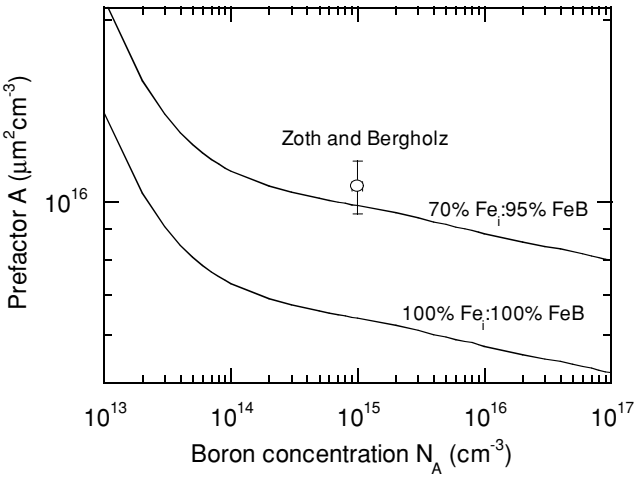

FIGURE 7. Pre-factor A for determining the absolute iron concentration in iron-dominated samples as a function of dopant density.

are curves calculated using Walz *et al.*'s values for the energy level and cross-sections of FeB pairs.

An important consideration in calculating such curves is the proportion of the total iron concentration in the form of Fe_i or FeB pairs. Even after thermal annealing, not all FeB pairs dissociate, and some will re-pair during cooling down. Zoth and Bergholz estimated that for their samples, about 70% of the available iron was present as Fe_i after the thermal treatment. Similarly, not all the iron will re-pair after a finite period of time at room temperature. The re-pairing rate is dependent on the boron concentration[2,18], and there may be as much as 5% interstitial iron in higher resistivity samples even after long periods of resting in the dark. Our data in Table 2 shows that some samples without light-soaking had only 80-90% of the iron present as FeB pairs, although they were not rested for long periods of time, and so are not directly comparable to Zoth and Bergholz's samples in terms of relative populations. Further, SPV measurements are performed under very low injection, whereas the QSSPC measurements performed here are generally around mid-injection. These higher carrier concentrations can cause FeB pair splitting, resulting in more interstitial Fe in our non light-soaked measurements than in Zoth and Bergholz's.

To illustrate the effect of these variations, Figure 6 shows the curves calculated for three different conditions: 100% Fe_i after annealing and 100% FeB before (ideal state, shown as 100%:100%); 70% Fe_i after annealing and 100% FeB before (shown as 70%:100%); and 70% Fe_i after annealing and 95% FeB before (shown as 70%:95%). This final condition is probably a good approximation of the relative populations in Zoth and Bergholz's samples, and yields good agreement with their data when using the cross-sections and energy levels used in this work. The curves reveal the importance of careful sample treatment when dissociating FeB pairs, as slight changes in relative populations can impact heavily on the results. Note that the curves from Walz's parameters do not follow the trend of Zoth's data, and are essentially flat, reflecting the fact that the low-injection lifetime for Walz's FeB center is independent of the dopant density, in contradiction to the experimental evidence presented here.

The curves in Figure 6 can be used to determine if a sample is dominated by iron. Zoth and Bergholz went on to show that in such cases, the absolute iron concentration can be determined by the following relation:

$$[Fe] = A \times \left(\frac{1}{L_1^2} - \frac{1}{L_0^2} \right) \qquad (3)$$

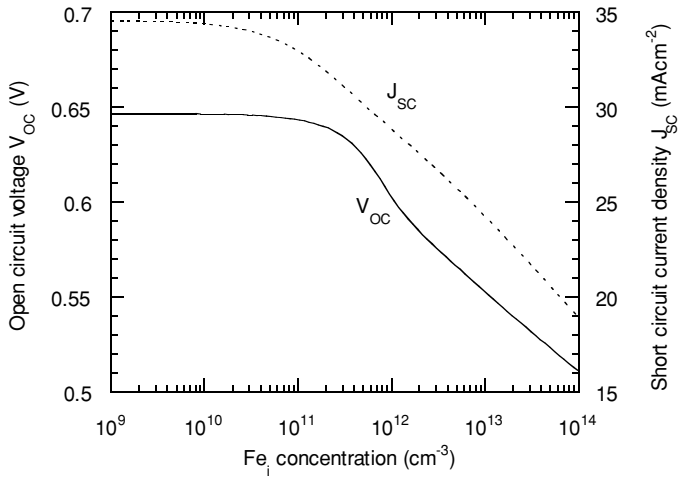

FIGURE 8. Effect of Fe_i concentration on V_{OC} and J_{SC} as modeled for a 1.5Ωcm cell of thickness 0.03cm and with $J_{0e}=3\times10^{-13}$ A/cm^2.

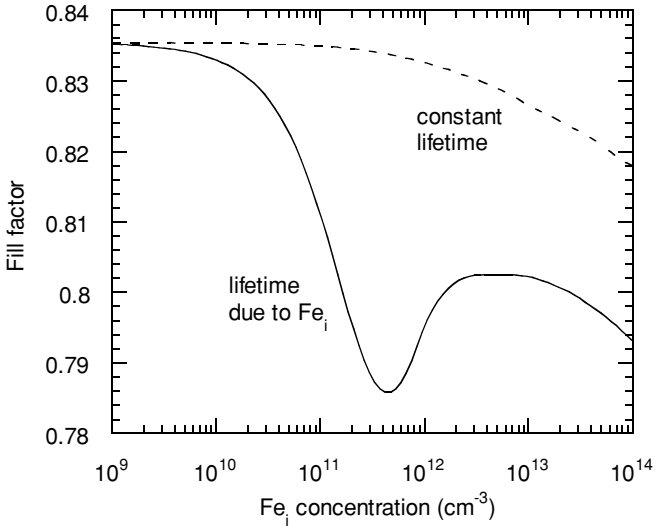

FIGURE 9. Effect of Fe_i concentration on fill factor. Also shown is the fill factor curve for a recombination centre that has an injection-level independent bulk lifetime (which is equal to the high-injection lifetime of Fe_i).

The diffusion lengths must be in microns, and the computed iron concentration is in cm^{-3}. The pre-factor A was found by Zoth and Bergholz to be 1.06×10^{14}cm^{-3} for samples with $N_A=10^{15}$cm^{-3}, although their value is often applied to wafers of different resistivities. Using the cross-sections and energy level found in this chapter, it is possible to calculate this pre-factor accurately for *any* resistivity. The result is shown in Figure 7, as well as Zoth and Bergholz's single data point. The 70% Fe_i after anneal:95% FeB before anneal curve falls within 10% of Zoth's data, and extends it to a large range of dopant densities.

4. IMPACT OF Fe_i ON SILICON SOLAR CELLS

In an illuminated silicon cell, any non-precipitated Fe will occur in the interstitial state. Using the recombination parameters in Table 1, it is possible to model the effect of Fe_i on the performance parameters of a cell [19] using PC1D [20]. Figure 8 shows the impact of differing levels of interstitial Fe on V_{OC} and J_{SC} modeled for a 1.5Ωcm cell of thickness 0.03cm, and with an emitter characterised by a saturation current density of $J_{0e}=3.0\times10^{-13}$A/cm^2. 85% of the incoming light is assumed to be coupled into the cell. The results show that for Fe_i concentrations below 10^{10}cm^{-3}, the voltage of such a cell is dominated totally by the emitter, which caps the V_{OC} at 647mV. Also, the short circuit current is essentially independent of the Fe concentration at these low Fe levels because the bulk diffusion length is many times longer than the cell thickness. As the interstitial Fe concentration increases, the current begins to fall as the low-injection diffusion length decreases below the cell thickness. V_{OC} begins to drop also as the lifetime at open circuit decreases. Note that the V_{OC} curve shows a 'kink' which is caused by the injection-level dependence of the bulk lifetime producing an accelerated decrease in the open circuit lifetime as the recombination center density increases. This kink is absent from the J_{SC} curve, because the low-injection lifetime never experiences any injection-level dependence, even at very high iron concentrations.

Of more interest however is the behaviour of the fill factor, which is shown in Figure 9. For very low Fe_i levels, the injection-level dependence of the effective lifetime, being dominated by the emitter, is very slight, and results in an ideal fill factor of 0.835. As the Fe_i concentration increases though, the fill factor begins to degrade due to the increasing SRH dependence around maximum power point. At around 5×10^{11}cm^{-3} Fe_i concentration, the strongest part of the SRH dependence is centered near one-sun maximum power conditions, limiting the fill factor to 0.785. As

the Fe_i level increases further still, the lifetime becomes low enough to take the one-sun carrier density below the strongest SRH dependence, and the fill factor begins to recover. At these high Fe_i levels however, the voltage and current drop off very quickly due to the decreasing magnitude of the bulk lifetime.

As the Fe_i concentration increases above $1\times10^{13}cm^{-3}$, the decreasing magnitude of the open circuit voltage causes the 'ideal' fill factor to decrease also, a well-known property of *p-n* junction diodes[21]. Naturally, this effect occurs even for the case where the lifetime is injection-level *in*dependent, as shown in the figure.

The underlying reason for the dramatic injection-level dependence of the SRH lifetimes for Fe_i, and hence the poor fill factors, is the large asymmetry between the electron and hole capture cross-sections, which differ by about three orders of magnitude.

5. CONCLUSIONS

Injection-level dependent lifetime measurements can provide an accurate way of determining capture cross-sections of recombination centers. An important aspect of the method is that several samples of widely different resistivities are needed to generate reliable results. In this work, the technique was applied to the acceptor level of FeB pairs in silicon.

These cross-sections allow the recombination dynamics of Fe_i/FeB-pair systems to be accurately predicted. As an example, it is possible to determine the resistivity-dependence of the pre-factor often used to determine the Fe concentration in wafers via the difference in diffusion lengths before and after dissociation. This resistivity dependence is often overlooked.

Finally, the large asymmetry between the cross-sections of Fe_i centers results in strongly injection-level dependent lifetimes, which in turn produce low fill factors, as well as the expected drop in voltage and current.

ACKNOWLEDGEMENTS

The authors are grateful to J. Wong-Leung for ion implantations, M. Kerr for SiN depositions and C. Jagadish for helpful advice. This work has been supported by the Australian Research Council.

REFERENCES

[1] A. A. Istratov, H. Hieslmair and E. R. Weber, *Appl. Phys. A* **69** 13-44 (1999).
[2] G. Zoth and W. Bergholz, *J. Appl. Phys.* **67** 6764-6771 (1990).
[3] S. D. Brotherton, P. Bradley and A. Gill, *J. Appl. Phys.* **57** 1941-1943 (1985).
[4] Y. Hayamizu, T. Hamaguchi, S. Ushio and T. Abe, *J. Appl. Phys.* **69** 3077-3081 (1991).
[5] D. Walz, J.-P. Poly and G. Kamarinos, *Appl. Phys. A* **62** 345-353 (1996).
[6] S. Rein, T. Rehrl, J. Isenberg, W. Warta and S. W. Glunz, 'Lifetime spectroscopy in silicon solar cells' *Proc. 16th Euro. Photovoltaic Solar Energy Conf.* Glasgow, U.K. 1476-1481 (2000).
[7] D. Macdonald, A. Cuevas and J. Wong-Leung, *J. Appl. Phys.* **89** 7932-7939 (2001).
[8] J. Schmidt and M. Kerr, *Sol. Energy Mater. Sol. Cells* **65** 585-591 (2000).
[9] R. A. Sinton and A. Cuevas, *Appl. Phys. Lett.* **69** 2510-2512 (1996).
[10] W. Shockley and W. T. Read, *Phys. Rev.* **87** 835-842 (1952).
[11] R. N. Hall, *Phys. Rev.* **87** 387 (1952).
[12] J. S. Blakemore, *Semiconductor Statistics*, International Series of Monographs on Semiconductors, Vol. 3, Pergamon Press, Oxford (1962).
[13] W. M. Bullis and H. R. Huff, *J. Electrochem. Soc.* **143** 1399-1405 (1996).
[14] J. Dziewior and W. Schmid, *Appl. Phys. Lett.* **31** 346-348 (1977).
[15] P. P. Altermatt, J. Schmidt, G. Heiser and A. G. Aberle, *J. Appl. Phys.* **82** 4938-4944 (1997).
[16] S. W. Glunz, D. Biro, S. Rein and W. Warta, *J. Appl. Phys.* **86** 683-691 (1999).
[17] R. A. Sinton and R. M. Swanson, *IEEE Trans. Elec. Dev.* **34** 1380-1389 (1987).
[18] H. Lemke, *Phys. Status Solidi A* **64** 215-224 (1981).
[19] D. Macdonald and A. Cuevas, *Prog. in Photovoltaics* **8** 363-375 (2000).
[20] P. A. Basore and D. A. Clugston, *PC1D V5.3*, University of New South Wales, Sydney, Australia (1998).
[21] M. A. Green, *Solar cells*, The University of New South Wales, Kensington, NSW (1998).